Pure & Appl. Chem., Vol. 52, pp.73-92.
Pergamon Press Ltd. 1979. Printed in Great Britain.

ON SULFIDES AND PNICTIDES

E. F. Bertaut

Laboratoire de Cristallographie, C.N.R.S., 166 X, 38042 Grenoble Cedex, France, et
Laboratoire de Diffraction Neutronique, C.E.N.G., 85 X, 38041 Grenoble-Cedex, France.

Abstract. - The three known varieties of FeS are described and some peculiar features of iron sulfide chemistry are discussed. One introduces the new tool of "similarity operators" for the study of the displacive transitions of FeS (T_α transition) and of MnAs (MnP $\rightleftarrows$ NiAs type). In pnictides the transitions magnetic $\rightarrow$ non magnetic (MnP type) are first order in conformity with observed changes of volumes and of transition temperatures versus pressure and/or concentration.

INTRODUCTION

All of you know the joke that "chemists are living in direct space, physicists in impulsion - or reciprocal space and that they should meet more frequently". Not only this is the case here, but fortunately we have some crystallographers present who connect both spaces by a Fourier* transform. When I had chosen the title which you see in the program, my intention was to give a general survey. But in view of the very abundant (and often contradictory) literature in that broad field -and this introduces already the lecture of Professor Kjekshus- I have restricted my talk to the study of some examples which in spite of the simple chemical formulae show already the complexity of the physical situation. The presence of a magnetic structure will turn out to be as significant as its absence and a newcomer in modern physics and crystallography, the charge density wave, will show its importance.

1. FeS VARIETIES

There is an incredible richness hidden in a chemical formula like FeS and for its interpretation we shall first rely on the simple Lewis-Kossel rules, say on rare gas like or full shell configuration.

1.1. Ionic case. In the ionic case, electron transfer takes place from a neutral atom 1 which becomes a cation to another neutral atom 2 which becomes an anion with well separated ions and no charge accumulation in between. When we write $Fe^{2+}X^{2-}$ we mean that we have transferred from $Fe(3d^64s^2)$ the two outer s electrons to the $X(ns^2np^4)$ atom in order to produce a rare gas configuration $X^{2-}(ns^2np^6)$. Here we meet already with a difficulty. Whilst a cation is always stable, a separate anion X^{2-} is unstable in a quantum mechanical calculation. Beforehand one must stabilize the anion X^{2-} by the positive potential produced by the ions of the lattice which is of cause the physical situation. Inversely the d-electrons of the cation feel the negative potential contribution of the neighbour anions. Ligand field theory is applicable : the degeneracy of the d electrons will be lifted partially or totally and the $10D_q$ effect will play an important role in an octahedral environment. The so-called "ionic" radii of the crystallographer will explain the interatomic distances.

1.2. Covalent case. When approaching two atoms, 1 and 2, again transfer of one electron takes place from atom 1 to atom 2, but also a transfer of one electron from atom 2 to 1. The two electrons form a spin compensated pair. There is a charge accumulation between the atoms which stay essentially neutral. (Only in the extreme case of the H_2 molecule there are charges + 1 on atoms 1 and 2 with a charge accumulation - 2 between the atoms). Ligand field theory is no longer applicable. Here the so-called "covalent" radii are used by crystallographers to explain interatomic distances which turn out to be much shorter than in the ionic case**. In that case the $Fe^{II}X^{II}$ species would be written Fe = X where = is the standard notation for a double bond, formed by four electrons, two from the Fe and two from the X atom.

* By the way, Fourier was "Préfet de Grenoble"
** To the knowledge of the author, there is no quantum mechanical proof, presently available, why "covalent" distances should be shorter than "ionic" distances.

The result is a full d^{10} shell, a spin compensated configuration around Fe.

Whilst figures 1a and b describe the two extreme possibilities of the FeS "molecule", the figures 2a and b represent the respective formulations $Fe^{2+}(S_2)^{2-}$ (ionic) and $Fe\begin{smallmatrix}S\\S\end{smallmatrix}$ (covalent) of FeS_2 (pyrite, marcasite). Note that in the ionic as well as in the covalent case the transferred electrons are localized.

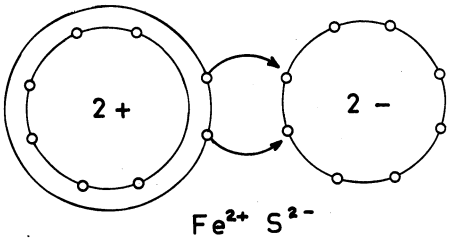

Fig 1a

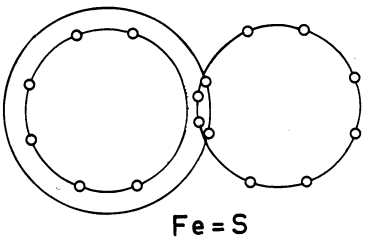

Fig 1b

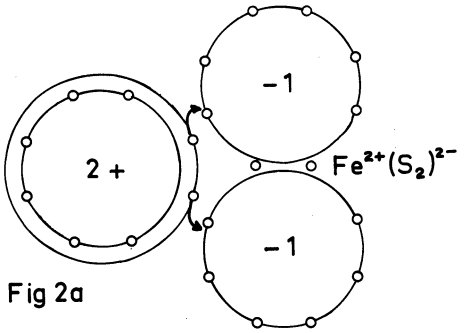

Fig 2a

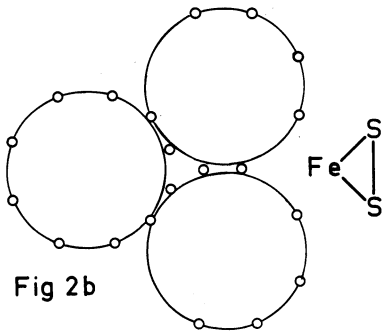

Fig 2b

Fig. 1 FeS
1a Ionic case
1b Covalent case

Fig. 2 FeS_2
2a Ionic case
2b Covalent case

The subtitle of figures 1 and 2 could be as well the "dream of the (molecular) chemist". Not only is the situation "in between" the extremes a) and b) for molecules but in reality we have to do with crystals in which Fe-Fe and X-X interactions cannot be neglected. Furthermore nature gratifies us with crystalline varieties which "in statu nascendi" do not always represent the most stable form. There are three known varieties of FeS which are tetragonal (mackinawite), cubic (blende) and hexagonal (deformed NiAs type) at room temperature. Table 1 summarizes some of their relevant properties. In the tetragonal form (1) Fe has a tetrahedral environment, depicted in figure 3 with very short Fe-S distances of 2.23 Å and does not show any magnetic order down to 1.7 K nor any paramagnetic background in neutron diffraction diagrams (2). It also has the lowest isomer shift δ* and the highest percentage of 4s electrons (2). This corresponds to a strongly covalent situation so that ligand field theory is not applicable and a (ionic) $e_g^4 t_{2g}^2$ situation is highly improbable.

---

* δ is reported to a Co^{57} source imbedded in Rh.

TABLE 1. FeS

	Tetragonal	Blende	Hexagonal
	P4/nmm	$F\bar{4}3m$ F222	$P6_3/mmc$ $P\bar{6}2c$
d(Fe-Fe) in Å	2.664	3.78	3.00(2x) 3.73(4x)
d(Fe-S) in Å	2.23	2.34	2.49
V(300 K) in $Å^3$	34.15	39.8	30.1
T_N in K		230	598
T_α in K			420
δ*mm/sec	0.305	0.65	1.25
x in $4s^x$	∿38 %	30 %	19 %
μ in μ_B	0	3.45	3.6

* At 4 K and for a Co^{57} source in Rh.

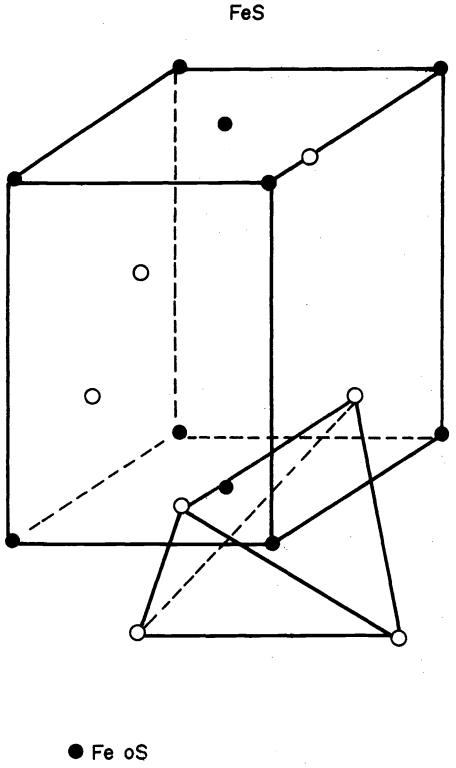

Fig. 3. FeS tetragonal

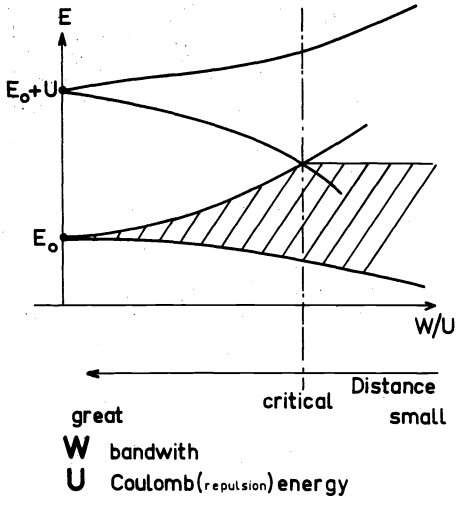

Fig. 4. Localized and Itinerant Electrons

1.3. Itinerant case and Tetragonal FeS. Time has come to discuss the situation of Fig. 4 (see also preceeding lecture). Here E_o is the energy of a first d electron and E_o + U the energy of a second d electron. U measures their Coulomb repulsion energy. To simplify one supposes that there is one d electron per site. At infinite distances of the atoms, the levels are discrete and only the lowest level ($E = E_o$) is occupied. When the atoms approach, two bands develop progressively, but the d electrons remain localized and order in some magnetic structure (ferromagnetic or antiferromagnetic Mott insulator) until a critical value of the parameter W/U is reached where the two bands merge into a single broad band and the electrons become itinerant (or delocalized)(3). Actually increasing W/U means decreasing distance. The very short Fe-Fe = 2.66 Å distance in tetragonal FeS is in favour of such an itinerant "spinless" situation.

We consider however that the question is not yet definitely settled. A cluster calculation for the (octahedral) complex FeS_6^{10} at distances d(Fe-S) = 2.5, 2.38 and 2.26 Å has shown that at d(Fe-S) = 2.28 Å a crossover of the quartet (high spin) and singlet (low spin) state (4) occurs or, expressed otherwise, sufficiently small metal chalcogenide distances are associated with highly covalent bonding and with spin pairing of d spins on the metal.

Thus we suggest a cluster calculation to be undertaken for the (tetrahedral) FeS_4^{-6} complex at various d(Fe-S) distances.

1.4. The form blende. In the form blende (space group $F\bar{4}3m$-T_d^2), Fe has again a tetrahedral environment. The Fe-Fe distances are considerable, 3.78 Å, and a localized high spin situation takes place. An antiferromagnetic collinear order (5) sets in at T_N = 234 K, accompanied by an orthorhombic (pseudo-tetragonal) distorsion (space group F222). The transition is first order*, as shown by a discontinuous jump of the hyperfine field at T_N (6) from 100 KOe to zero. The value at 0 K is 145 KOe. An analogous temperature variation is reported for the magnetic intensities (5). The magnetic structure is that of ferromagnetic layers stacked in a +-+-... sequence along the pseudo-tetragonal c-axis. The spins are along the longest axis a = 5.54 Å (b = 5.487 Å, c = 5.195 Å). The magnetic space group is $F_C22'2'$. As well in the blende as in the hexagonal form of FeS the Néel temperatures are much higher than in FeO ($\sim$ 180 K). This indicates a high overlap of d orbitals with anion p orbitals and the formation of antibonding orbitals $\psi\uparrow$ symbolically written

$$\psi\uparrow = N_A(d\text{-}Ap) \tag{1}$$

say a high value of A. A significant quantity is the overlap integral S(2)

$$S = \langle d|p\rangle \tag{2}$$

Exchange integrals (and Néel temperatures) are proportional to the fourth power of S. S can be appreciated by the magnetic moment reduction, measured by neutron diffraction, which goes as $1 - A^2 \simeq 1 - S^2$.

The reduction is here of about 14 %, but can reach much higher values (30 % in Cr_2NiS_4 (7), Cr_3S_4 (7) and (8). The mechanism of the spin reduction in antiferromagnets (Hubbard-Marshall (9)) is clear from equation (1). Spin is transferred from the cation to the anion, and as in most antiferromagnets the anion has an equal number of cations with plus and with minus spins as first neighbours, the transferred spins cancel on the anion.

Remark. This mechanism is still valid in ferrimagnets to a certain extent. In ferromagnets (and metamagnets near to ferromagnets like MnP) the observed spin reduction is not due to (1) but to either covalent spin paired bonding orbitals $\psi\uparrow\downarrow$

$$\psi\uparrow\downarrow = N_B(p + Bd) \tag{3}$$

or to the spinless (itinerant) situation mentioned above. In all cases one has

$$A = B + S \quad \text{and} \quad A > S \tag{4}$$

In (1) and (3), A and B stay for antibonding and bonding respectively ; N_A and N_B are normalization constants.

To summarize, overlap has antagonistic effects, increasing the exchange integral J, but decreasing the magnetic moment μ. In the energy expression, J and μ^2 vary like S^4.

1.5. Hexagonal FeS. Many papers have been written on hexagonal FeS which has a high Néel temperature, T_N = 598 K. It is a typical layer antiferromagnet formed of ferromagnetic + and - spin sheets alternating along the c-axis. The spins are in the c-plane between T_N and T_S = 445 K where they start rotating towards the c-axis in a temperature interval of about 25 degrees (10). Above T_α = 415 K the structure belongs to the NiAs type (space group G = $P6_3/mmc$) whilst at T_α a ("poor") metal to (small gap) semiconductor transition takes place (11)(12), accompanied by a deformation to space group g = $P\bar{6}2c$ (13)(14). At T_α the hyperfine field changes from 240 KOe in the NiAs phase to 300 KOe in the deformed phase and saturates at 323 KOe at 0 K (11)(15).

---

*The orthorhombic distorsion belongs to the irreducible representation Γ_3 of the site group $\bar{4}3m$-T_d of Fe and $[\Gamma_3]^3$ contains Γ_1 (Landau criterion).

Above 600 K(T_N) the metallic conductivity drops as in a normal metal and the magnetic moment seems to be higher than spin only (16) (μ_{eff} = 5.22 μ_B, $\mu_{eff}(S = 2)$ = 4.88 μ_B). At low temperatures the moment determined by neutron diffraction is about 3.57 μ_B (measured on a sample $Fe_{1-x}S$ with x = 0.098 and T_N = 600 K) (17).

The last line of table I corresponds to a crude estimation of x in $3d^6 4s^x$, expressed in %, according to the empirical relation (18)(19)(20) of Vincent and Shannon

$$x = - 78.7\ R + 86.6$$

where R is the ratio of the volumes of the FeS variety and of MgS, in qualitative agreement with the Walker and al. (W.W.J.) scale (21).

The tetragonal and blende forms of FeS are metastable and transform by heating irreversibly to the hexagonal form. The free energy will behave as in Fig. 5, showing a minimum at d_1 and a deeper minimum at $d_2 > d_1$. In spite of the increase of the distance Fe-S, the volume of FeS hexagonal is smallest, due to the increase from 4 to 6 of the coordination number.

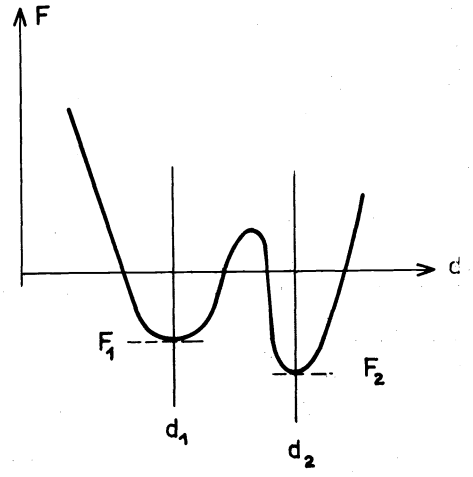

Fig. 5. Stability diagram : F = free energy ; d = distance

1.6. Valency states of Fe and of S, Se. There is no stable $Fe_2^{III}S_3$. Instead of allowing oxidation from Fe^{II} to Fe^{III}, the X ions (X = S, Se, Te) prefer to attain a X^- configuration, say to have a hole in the valence band (22)(23). If the concentration of X^- ions is sufficient they may condense to $(X_2)^{2-}$ as they do in FeS_2.

In a selenide like Fe_3Se_4 (24) (space group I2/m, a = 6.20 Å, b = 3.53 Å, c = 11.26 Å, β = 91°44 at 350 K), the formula at the temperature of preparation (hydrothermal synthesis under reducing conditions at 350°C) is probably (25)

$$Fe_3^{2+x}(Se^{2-})_2(Se^-)_2e^{-3x}$$

and, at low temperatures, seems to correspond to

$$Fe^{III}Fe_2^{II}(Se^{2-})_3Se^-$$

but without attaining

$$Fe_2^{III}Fe^{II}Se_4^{2-}.$$

Neutron diffraction measures a magnetic moment of 3.25 μ_B on the site 2c) and 1.94 μ_B on the site 4i) (24) while the hyperfine fields measured by the Mössbauer effect are 240 and 112 KOe respectively (26) in this ferrimagnet. The Se-Fe distances are exceedingly short (Se_I has 4 neighbours Fe at the average distance of 2.42 Å and Se_{II} has 5 neighbours Fe at the average distance of 2.52 Å) which is in favour of the presence of the Se^- species. The considerable reduction of the moment and hyperfine field is in favour of highly covalent effects.

In the same spirit, the pyrrhotite formula could well be near to $Fe_7^{2+x}\square S_2^{-}S_6^{2-}e^{-7x}$ (x corresponds to delocalized electrons).

Mössbauer effect studies see an isomer shift corresponding to Fe^{2+} (27)(28) in reasonable agreement with nearly equal average distances FeS in the octahedra around the four present iron species, say 2.446 ; 2.449 ; 2.456 ; 2.444 Å for the species Fe_1, Fe_2, Fe_3, Fe_4 (29). We find however that the S_j-Fe distances in the polyhedra around S_j (j = 1, 2, 3, 4) show significant differences. In the normal prismatic Fe_6 environment of S_4, the average distances d(S-Fe) is 2.57 Å, near to the distance of 2.58 Å, calculated with the Ahrends radii of Fe^{2+} and S^{2-} whilst the average S-Fe distance in the $Fe_5\square$ environment of S_3 is definitely shorter and equal to 2.37 Å. This is in favour of the interpretation that the species S_3 is near to a S^{-} configuration (25).

Stabilization of Fe^{III}. The contribution to the electrostatic energy of a species j is $\frac{1}{2}q_jV_j$ and a cation j will show its highest valency state q_j when the potential V_j at its location j is as negative as possible. The stabilization of Fe^{III} and more generally of high valency states of transition metal cations is a "second shell effect". Whilst the first shell formed by the anions produces a negative potential at the cation location, the second shell formed by cations counteracts this potential by a positive contribution.

Three factors will favour high valency states.

i) the second shell cation shows a high difference of electronegativity with the anion so that electron transfer from the second shell cation to the first shell anions will be complete and enhance $|V_j|$

ii) the second shell cation is big (distance effect in 1/r) and

iii) its valency is small.

Effects ii) and iii) will minimize the positive contribution to the potential at the cation j.

For instance, reasons i) and ii) stabilize Co^{3+} in $LaCoO_3$; i), ii) and iii) stabilize tetrahedral Fe^{III} in $KFeS_2$ and $CuFeS_2$. It should be added however that in all instances the moments reported for Fe^{III} are small : 3.85 μ_B in $CuFeS_2$ (30) and 2.43 μ_B in $KFeS_2$ (31) at 4.2 K, which is a one-dimensional antiferromagnet. Also the hyperfine field is small, 215 KOe in $KFeS_2$ (32) and the isomershift indicates a 0.35 contribution from the ligand to the 4s orbital so that the total charge on "Fe^{III}" is 3 - 4 x 0.35 = 1.6. The best fit with a point charge model is obtained for q(S) = - 1.3 and q(Fe) = 1.6 (32).

Intermediate valency states. In cubanite $CuFe_2S_3$ which is a semiconductor (33), the two iron atoms are equivalent as proven by a unique Mössbauer spectrum (34). The structure contains iron atom by pairs : each iron has a tetrahedral environment and two tetrahedra share one edge so that the Fe-Fe distance is small, 2.8 Å. The magnetic structure in which there are plus and minus pairs of spins along the a axis (see figure 6) (35), confirms the model, suggested in reference (36). This model was also compatible with representation theory and with the existence of a weak ferromagnetic component along b (37) which extrapolates to 0.04 μ_B at low temperatures. In the antiferromagnetic mode the moment value per iron is 3.2 μ_B. A polarized neutron study (38) eliminates the possibility of any moment on the copper atom which is in a Cu^{+} state. A recent study of the spin density, undertaken in our laboratory shows the form factor of Fe in cubanite to be near to that of Fe^{3+} and far from that of Fe^{2+} (39) (see figure 7). Thus one must conclude that the valency state is $Fe^{2.5+}$ and that in a pair of tetrahedra the Fe atoms share an e_g electron (38).

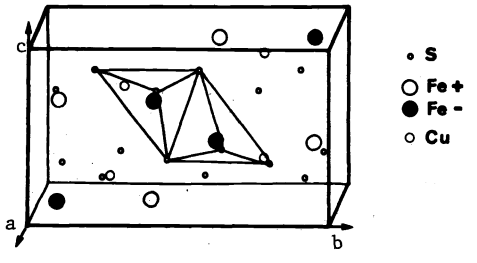

Fig. 6. Magnetic structure of $CuFe_2S_3$

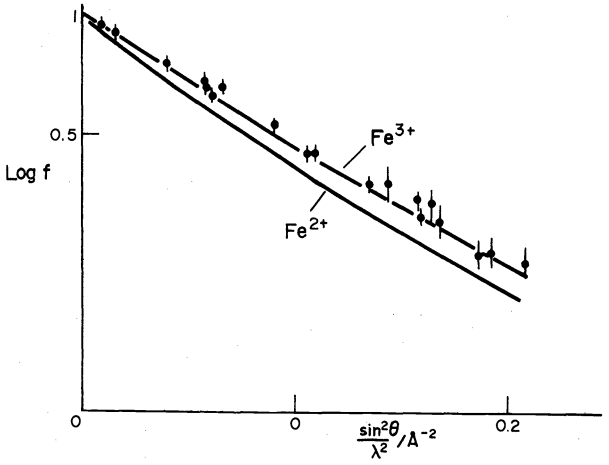

Fig. 7. Magnetic Fe form factor in $CuFe_2S_3$

In view of the lack of neutron and magnetic data we only mention the "infinitely adaptive" series of iron barium sulfides like $Ba_{1+x}Fe_2S_4$ and others (40) in which chains of edge sharing Fe-S tetrahedra run along a crystal axis, barium being accommodated between the chains with a periodicity which may be different from that of the iron chains (chage density waves) (41).

2. SIMILARITY OPERATORS AND PHASE TRANSITIONS

After this short review of some problems of iron sulfide chemistry, let us return to the firm ground of crystallography.

We shall show that the knowledge of the group G at high temperature on one hand, and of the relations between the parameters of the unit cells at high and low temperatures on the other hand restricts considerably the choice of the subgroup g at low temperature.

We shall first recall the theory of similarity operators, a new mathematical tool we have developed recently (42)(43). Similarity operators connect operators and atomic positions in the subgroup to those of the group and will show to be useful in phase transitions. We shall apply this theory to the T_α transition of FeS and also to the crystallographic high temperature transition of MnAs from the NiAs to the MnP type structure.

2.1. Theory. Definitions. Let G be a space group described in the reference frame (O, $\underset{\sim}{A}$, $\underset{\sim}{B}$, $\underset{\sim}{C}$). Here O is the origin of the translation lattice and $\underset{\sim}{A}$, $\underset{\sim}{B}$, $\underset{\sim}{C}$ are the vectors defining the unit cell. A symmetry operator in G will be written (Koster-Seitz notation)

$$\underline{a} = (\alpha|\tau_\alpha) \tag{5}$$

Let g be a subgroup of G described in the reference frame (o, $\underset{\sim}{a}$, $\underset{\sim}{b}$, $\underset{\sim}{c}$). Here o is the origin of the translation lattice and $\underset{\sim}{a}$, $\underset{\sim}{b}$, $\underset{\sim}{c}$ are the vectors defining the unit cell in g. A symmetry operator in g will be written

$$\underline{b} = (\beta|\tau_\beta) \tag{6}$$

One has the "lattice relation"

$$(\underset{\sim}{a}, \underset{\sim}{b}, \underset{\sim}{c}) = (\underset{\sim}{A}, \underset{\sim}{B}, \underset{\sim}{C})S \tag{7}$$

Here ($\underset{\sim}{a}$, $\underset{\sim}{b}$, $\underset{\sim}{c}$) and ($\underset{\sim}{A}$, $\underset{\sim}{B}$, $\underset{\sim}{C}$) are row matrices and S is a 3 x 3 matrix.

We define a similarity operator S by

$$S = (S|\underset{\sim}{T}) \tag{8}$$

Here $\underset{\sim}{T}$ is the vector $\vec{Oo}$ which separates the origins O and o.

Properties of S. The atomic positions $\underset{\sim}{R}$ in G and $\underset{\sim}{r}$ in g are related by

$$\underset{\sim}{R} = S\underset{\sim}{r} = S\underset{\sim}{r} + \underset{\sim}{T} \tag{9}$$

The homologous symmetry operations $\underline{a}$ in G and $\underline{b}$ in g are related by

$$\underline{a}S = S\underline{b} \tag{10}$$

2.2. Application to the T_α transformation of FeS. The unit cell of the deformed hexagonal structure is defined by the parameters $a = A\sqrt{3}$ and $c = 2C$ where A and C are the parameters of the high temperature, a and c of the low temperature form (13). One has in vector notations

$$\underset{\sim}{a} = 2\underset{\sim}{A} + \underset{\sim}{B} \; ; \; \underset{\sim}{b} = -\underset{\sim}{A} + \underset{\sim}{B} \; ; \; \underset{\sim}{c} = 2\underset{\sim}{C} \tag{11}$$

The matrix S is consequently

$$S = \begin{pmatrix} 2 & -1 & 0 \\ 1 & 1 & 0 \\ 0 & 0 & 2 \end{pmatrix} \tag{12}$$

Its determinant is equal to 6 so that the translation group of g, the low temperature group is a subgroup of index 6 of the translation group of the high temperature group $G = P6_3/mmc$ (NiAs type).

The inverse of S is

$$S^{-1} = \begin{pmatrix} \frac{1}{3} & \frac{1}{3} & 0 \\ -\frac{1}{3} & \frac{2}{3} & 0 \\ 0 & 0 & \frac{1}{2} \end{pmatrix} \tag{13}$$

The reciprocal vectors are calculated either directly or by observing that

$$\begin{pmatrix} \underset{\sim}{a}^* \\ \underset{\sim}{b}^* \\ \underset{\sim}{c}^* \end{pmatrix} = S^{-1} \begin{pmatrix} \underset{\sim}{A}^* \\ \underset{\sim}{B}^* \\ \underset{\sim}{C}^* \end{pmatrix} \tag{14}$$

One finds

$$\begin{aligned} \underset{\sim}{a}^* = \underset{\sim}{g}_1 &= \tfrac{1}{3}(\underset{\sim}{A}^* + \underset{\sim}{B}^*) = [\tfrac{1}{3}, \tfrac{1}{3}, 0] \\ \underset{\sim}{b}^* = \underset{\sim}{g}_2 &= \tfrac{1}{3}(-\underset{\sim}{A}^* + 2\underset{\sim}{B}^*) = [-\tfrac{1}{3}, \tfrac{2}{3}, 0] \\ \underset{\sim}{c}^* = \underset{\sim}{g}_3 &= \tfrac{1}{2}\underset{\sim}{C}^* = [0, 0, \tfrac{1}{2}] \end{aligned} \tag{15}$$

2.2.1. Search of the subgroup g of $G = P6_3/mmc$. The subgroup g of the deformed FeS structure must admit the translation lattice, constructed on the vectors $\underset{\sim}{a}$, $\underset{\sim}{b}$, $\underset{\sim}{c}$ and have at least trigonal symmetry. We proceed stepwise by looking for maximal subgroups*.

We start with the non centrosymmetric subgroups of index 2 of G and shall consider later on the centrosymmetric ones.

Maximal non centrosymmetric subgroups of G. These are $P6_3mc$, $P6_322$, $P\bar{6}2c$ and $P\bar{6}m2$. The next step is to find for these four space groups the subgroups which admit the unit cell parameters $A\sqrt{3}$, $A\sqrt{3}$, C. They are of index 3 and in the order of the sequence above $P6_3cm$, $P6_322$, $P\bar{6}c2$ and $P\bar{6}2m$. The final step is to see if these four groups admit subgroups of index two in which the dimension along Oz is doubled, say $\underset{\sim}{c} = 2\underset{\sim}{C}$. There is none except for $P\bar{6}2m$ which admits two subgroups : $P\bar{6}2m$ (isosymbolic) and $P\bar{6}2c$ which are of index 2 x 3 x 2 = 12 with respect to G. We could have inverted the two last steps, by looking first for the subgroups of index two (C doubling) and second for those of index 3 with the same result.

Maximal centrosymmetric subgroups of G. These are $P\bar{3}m1$ and $P\bar{3}1c$, of index two and admit themselves maximal subgroups of index 3 (with unit cell parameters $A\sqrt{3}$, $A\sqrt{3}$, C) which are $P\bar{3}1m$ and $P\bar{3}c1$ respectively. Only $P\bar{3}1m$ admits C doubling and its final maximal subgroups of index 12 with respect to G are $P\bar{3}1m$ (isosymbolic) and $P\bar{3}1c$.

The diffraction experiment clearly indicates the existence of a glide plane $\underline{c}$ so that $\underline{P\bar{6}2c}$ and $\underline{P\bar{3}1c}$ are the only candidates.

The procedure is not unique but the result is. We could have started with the (unique) maximal subgroup of index 3 of G, having the translation lattice parameters $A\sqrt{3}$, $A\sqrt{3}$, C which is $P6_3/mcm$. One would then have to choose among the subgroups of $P6_3/mcm$ those which allow doubling in the C-direction. They are $\underline{P\bar{3}1m}$ and $\underline{P\bar{6}2c}$ as in the discussion above.

2.2.2. Homologous symmetry operators and point positions. In the NiAs type structure one has Fe in 2a : 0 0 0, 0 0 $\frac{1}{2}$ and S in 2c : $\frac{1}{3}\ \frac{2}{3}\ \frac{1}{4}$; $\frac{2}{3}\ \frac{1}{3}\ \frac{3}{4}$. FeS deformed has the space group $g = P\bar{6}2c$ in which the generators are the lattice translations $\underset{\sim}{a}$, $\underset{\sim}{b}$, $\underset{\sim}{c}$ and the following choice of $\underline{b}$ operators

$$\underset{\sim}{\bar{6}} = (6_z|0\ 0\ \tfrac{1}{2}) \ ; \ \underset{\sim}{2} = (2'_x|0\ 0\ 0) \tag{16}$$

Remark. The operator $\underset{\sim}{c}$ is not independent. One has

$$\underset{\sim}{c} = \underset{\sim}{\bar{6}}.\underset{\sim}{2} = (m''|0\ 0\ \tfrac{1}{2}) \tag{16a}$$

Here we have abbreviated

$$\bar{6}_z = \begin{pmatrix} -1 & 1 & 0 \\ -1 & 0 & 0 \\ 0 & 0 & -1 \end{pmatrix} \ ; \quad 2'_x = \begin{pmatrix} 1 & -1 & 0 \\ 0 & -1 & 0 \\ 0 & 0 & -1 \end{pmatrix} \ ; \quad m'' = \begin{pmatrix} -1 & 0 & 0 \\ -1 & 1 & 0 \\ 0 & 0 & 1 \end{pmatrix} \tag{17}$$

---

* They will be given explicitly in the new edition of International Tables (44)

The choice of $\underset{\sim}{T}$, say the origin o in g, is by no means trivial. We study here the case (see figure 8)

$$T = \frac{1}{3}\ \frac{2}{3}\ \frac{1}{4} \tag{18a}$$

which means physically that o is taken on the S atom. If the theory, presented here, is correct, one should find from the operators $\underline{b}$ above the homologous operators $\underline{a}$ in G by

$$\underline{a} = S\underline{b}S^{-1} \quad \text{where } S^{-1} = (S^{-1}|-S^{-1}T) \tag{19}$$

One finds indeed by straightforward calculations the following $\underline{a}$ operators in G :

$$\underset{\sim}{\bar{6}} = (\bar{6}_z|0\ 1\ \tfrac{3}{2}) \ ;\ \underset{\sim}{2}'' = (2''|0\ 1\ \tfrac{1}{2}) \ ;\ \underset{\sim}{m}' = (m'|1\ 0\ 0) \tag{20}$$

Here we have used the abbreviations

$$m' = \begin{pmatrix} 0 & -1 & 0 \\ -1 & 0 & 0 \\ 0 & 0 & 1 \end{pmatrix} \quad ; \quad 2'' = \begin{pmatrix} 1 & 0 & 0 \\ 1 & -1 & 0 \\ 0 & 0 & -1 \end{pmatrix} \tag{21}$$

As usually 2' indicates a twofold axis of the first kind (along the axis), 2" a twofold axis of the second kind (orthogonal to the axis) ; m' and m" are mirror operations of the first and second kind respectively.

It is easily checked that $\underset{\sim}{m}'_1$ and $\underset{\sim}{2}''$ keep the point $\frac{1}{3}\ \frac{2}{3}\ \frac{1}{4}$ invariant, whilst $\underset{\sim}{\bar{6}}$ (see above) leave invariant the point $\frac{1}{3}\ \frac{2}{3}\ \frac{3}{4}$. A glance on the International Tables shows that in $P6_3/mmc$ the site symmetry of $S(\frac{1}{3}\ \frac{2}{3}\ \frac{3}{4})$ is $\bar{6}m2$. Thus it is quite instructive to see that the $\bar{6}$ operator which keeps $\frac{1}{3}\ \frac{2}{3}\ \frac{1}{4}$ invariant, say $(\bar{6}_z|0\ 1\ \frac{1}{2})$ has disappeared when passing from G to g.

Position vectors in G and g. From (9) one gets

$$\underset{\sim}{r} = S^{-1}(\underset{\sim}{R} - \underset{\sim}{T}) \tag{22}$$

Fe positions. One could choose $\underset{\sim}{R} = 0\ 0\ 0$. However for convenience we consider the equivalent point $\underset{\sim}{R}(Fe) = 1\ 1\ \frac{1}{2}$ so that the coordinates of $\underset{\sim}{r}$ become positive in g

$$\underset{\sim}{r}(Fe) = \frac{1}{3}\ 0\ \frac{1}{8}, \text{ general position (12i) in g.}$$

S positions. They split into three non equivalent positions

$$\underset{\sim}{R}(S) = \frac{1}{3}\ \frac{2}{3}\ \frac{1}{4} \rightarrow r(S_1) = 0\ 0\ 0, \ (2a)$$

$$\underset{\sim}{R}(S) = \frac{1}{3}\ \frac{2}{3}\ \frac{1}{4} + 0\ 1\ 0 \rightarrow r(S_2) = \frac{1}{3}\ \frac{2}{3}\ 0, \ (4f)$$

$$\underset{\sim}{R}(S) = \frac{2}{3}\ \frac{1}{3}\ \frac{3}{4} + 1\ 1\ 0 \rightarrow r(S_3) = \frac{1}{3}\ 0\ \frac{1}{4}, \ (6h) \text{ in g.}$$

The $\underset{\sim}{R}$ positions have been chosen so that the $\underset{\sim}{r}$ positions resemble those given in reference (13).

The reader may check that if one has chosen

$$T = 0\ 0\ \frac{1}{4} \tag{18b}$$

there would be three non equivalent positions of Fe of multiplicity 4 (4f twice and 4e) and two non equivalent S positions of multiplicity 6 (6g and 6h).

The present author confesses that the choice of the origin was a big problem for him when he analyzed the structure (13). Only recently one has become aware of the importance of this choice. The order of a transition may depend on the choice of the origin (45).

Discussion of $P\bar{3}1c$. Only T = 0 is possible. g has the generators $\underline{a}$, $\underline{b}$, $\underline{c}$ and

$$\underset{\sim}{\bar{3}} = (\bar{3}_z|0\ 0\ 0) \ ;\ \underline{c} = (m''|0\ 0\ \tfrac{1}{2})$$

The homologous operators in G are

$$\underset{\sim}{\bar{3}} = (\bar{3}_z|0\ 0\ 0) \ ;\ \underset{\sim}{m}' = (m'|0\ 0\ 1)$$

and the correspondence between positions reduces to

$$\underset{\sim}{r} = S^{-1}\underset{\sim}{R}$$

Fe positions would split into five positions 2a, 2b, 2c, 2d and 4f whilst S would occupy the general positions 12i in $P\bar{3}1c$.

In fact, Mössbauer effect studies alone prove already the equivalence of all Fe atoms (11). A fuller study of the small displacements of Fe (and S) atoms, alluded to in figure 9 will be given elsewhere (53).

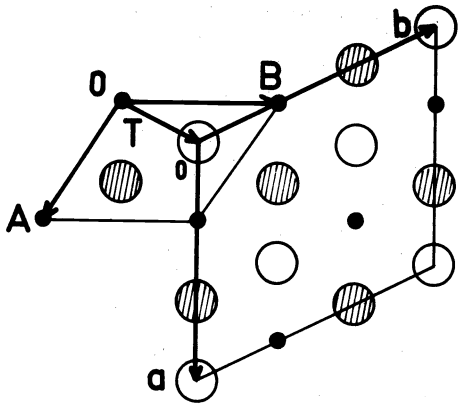

Fig. 8. FeS cells (see text)
0 = origin in the reference frame of $G=P6_3/mmc$

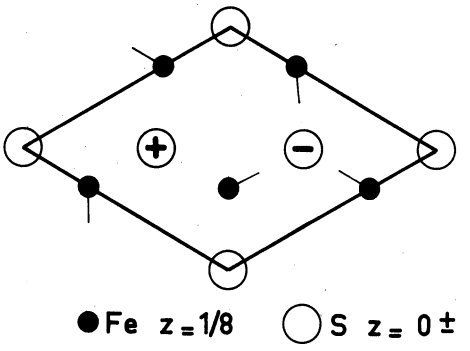

Fig. 9. Fe displacements below T_α

2.3. Application to the high temperature transition NiAs $\rightleftarrows$ MnP

2.3.1. Determination of the similarity operator. The geometrical relations between the NiAs ($\underset{\sim}{A}$, $\underset{\sim}{B}$, $\underset{\sim}{C}$) and MnP ($\underset{\sim}{a}$, $\underset{\sim}{b}$, $\underset{\sim}{c}$) structure types have been extensively described by Kjekshus and his coworkers (46) so that we shall only restate the main results in terms of the similarity operators. One has the vector relations

$$\underset{\sim}{a} = \underset{\sim}{C} \; ; \; \underset{\sim}{b} = \underset{\sim}{A} \; ; \; \underset{\sim}{c} = \underset{\sim}{A} + 2\underset{\sim}{B} \tag{23}$$

so that the matrix S and its inverse S^{-1} are given by

$$S = \begin{pmatrix} 0 & 1 & 1 \\ 0 & 0 & 2 \\ 1 & 0 & 0 \end{pmatrix} \quad ; \quad S^{-1} = \begin{pmatrix} 0 & 0 & 1 \\ 1 & -\frac{1}{2} & 0 \\ 0 & \frac{1}{2} & 0 \end{pmatrix} \tag{24}$$

The group of MnP is g = Pnma. One has :

$$\underset{\sim}{n} = (m_x|\tfrac{1}{2}\,\tfrac{1}{2}\,\tfrac{1}{2}) \; ; \; \underset{\sim}{m} = (m_y|0\,\tfrac{1}{2}\,0) \; ; \; \underset{\sim}{a} = (m_z|\tfrac{1}{2}\,0\,\tfrac{1}{2}) \tag{25}$$

where

$$m_x = \begin{pmatrix} -1 & 0 & 0 \\ 0 & 1 & 0 \\ 0 & 0 & 1 \end{pmatrix} \quad \text{etc...} \tag{26}$$

The generators above represent the operators $\underline{b} = (\beta|\tau_\beta)$ of g. We find the homologous operators $\underline{a} = (\alpha|\tau_\alpha)$ in G from (10), say explicitly

$$\begin{aligned} \alpha &= S\beta S^{-1} \\ \tau_\alpha &= S\tau_\beta + (1 - \alpha)T \end{aligned} \tag{27}$$

We put

$$\underset{\sim}{T} = X_o, \; Y_o, \; Z_o \tag{28}$$

and tabulate the results as follows

TABLE 2. Homologous Operators

Operators in g	Operators in G α	τ_α	$(\alpha\|\tau_\alpha)$
n →	$\begin{pmatrix} 1 & 0 & 0 \\ 0 & 1 & 0 \\ 0 & 0 & -1 \end{pmatrix}$	$1,1,\frac{1}{2}+2Z_o$	$= (m_Z\|1\ 1\ \frac{1}{2})$
m →	$\begin{pmatrix} -1 & 1 & 0 \\ 0 & 1 & 0 \\ 0 & 0 & 1 \end{pmatrix}$	$2X_o - Y_o + \frac{1}{2},0,0$	$= (m'_X\|0\ 0\ 0)$
a →	$\begin{pmatrix} 1 & -1 & 0 \\ 0 & -1 & 0 \\ 0 & 0 & 1 \end{pmatrix}$	$\frac{1}{2}+Y_o,\ 1+2Y_o,\ \frac{1}{2}$	$= (m''\|0\ 0\ \frac{1}{2}) = c$

Here m'_X is a mirror or the first kind, perpendicular to $\underset{\sim}{A}$ and m" is a mirror of the second kind, containing $\underset{\sim}{A}$. The last column contains the symbols of the operators $(\alpha|\tau_\alpha)$ so that the components of $\underset{\sim}{T}$ are obtained by simple identification (origin o in g) as

$$X_o = -\frac{1}{2}\ ,\ Y_o = -\frac{1}{2},\ Z_o = 0 \tag{29}$$

The position vectors $\underset{\sim}{r}$ in g are obtained from

$$\underset{\sim}{r} = S^{-1}\underset{\sim}{R} + o\ \frac{1}{4}\ \frac{1}{4}$$

Thus

$\underset{\sim}{R}$ = 0 0 0 in G corresponds to $\underset{\sim}{r} = o\ \frac{1}{4}\ \frac{1}{4}$ in g, to be compared to 0.005, $\frac{1}{4}$, 0.222 for Mn.

$\underset{\sim}{R} = \frac{1}{3}\ \frac{2}{3}\ \frac{1}{4}$ in G corresponds to $\underset{\sim}{r} = \frac{1}{4}\ \frac{1}{4}\ \frac{7}{12}$ in g, to be compared to 0.224, $\frac{1}{4}$, 0.582 for As in MnAs (7/12 = 0.583) (47) (values extrapolated to 298 K).

2.3.2. Displacement modes by representation analysis. The author has given some ten years ago a theory of non collinear ferroelectrics and antiferroelectrics which is able to enumerate all possible displacement modes when the space group G and the wave vector q are known (48). This theory[+] applies of course to the so called "modulated structures" to which presently much attention is devoted. They are just antiferroelectrics. Here the notion of the wave vector group G_q is important. By definition only those operators $\underline{a}$ of the group G survive in the group G_q for which

$$\alpha_t \underset{\sim}{q} = \underset{\sim}{q} + \underset{\sim}{Q} \tag{30}$$

Here $\underset{\sim}{q}$ is a vector of reciprocal space and $\underset{\sim}{Q}$ a vector of the reciprocal lattice of G ; α_t is the transpose of α, the rotational part of $\underline{a}$ (5).

We shall enumerate all displacement modes, possible in G_q and compare them with the small displacements, inferred from the use of similarity operators. As an example we choose the MnP structure, considered as a "displacement mode" of the NiAs structure. The treatment is given in full to illustrate the simplicity of the method (48)(49).

Applying (14), the reciprocal lattice vectors of the MnP lattice are

$$\underset{\sim}{a}^* = \underset{\sim}{C}^*\ ;\ \underset{\sim}{b}^* = \underset{\sim}{A}^* - \frac{1}{2}\underset{\sim}{B}^*\ ;\ \underset{\sim}{c}^* = \frac{1}{2}\underset{\sim}{B}^* \tag{31}$$

Here the wave vector $\underset{\sim}{q}$ appears

$$\underset{\sim}{q} = \frac{1}{2}\underset{\sim}{B}^* = [0\ \frac{1}{2}\ 0] \tag{32}$$

One has for instance

$$(2'_x)_t = \begin{pmatrix} 1 & 0 & 0 \\ -1 & -1 & 0 \\ 0 & 0 & -1 \end{pmatrix} \quad \text{and} \quad (2'_x)_t \cdot \underset{\sim}{q} = \begin{pmatrix} 0 \\ -\frac{1}{2} \\ 0 \end{pmatrix} = \underset{\sim}{q} + \begin{pmatrix} 0 \\ -1 \\ 0 \end{pmatrix} \tag{33}$$

[+]The theory is analogous to the representation analysis outlined for magnetic structures (50) (37). The only difference is that in the magnetic case one has to do with axial vectors (spins, orbital moments) whilst in the electric counterpart one studies polar vectors, say moments which are products of a charge by a displacement. Displacements are polar vectors.

which satisfies (30) (whilst $\bar{6}$, $(\bar{6})^2$, 6_3, $(6_3)^2$ do not). Finally G_q has the following symmetry operations a in common with G : the twofold rotations 2_x, the helical rotation $2_{1z} = (6_3)^3$, the inversion $\bar{1}$ and their products so that the full notation of G_q is $\underline{P2/m}\ 2/\underline{c}\ 2_1/\underline{m}$ (= $\underline{Pmcm}$) in the reference frame of G. Thus the x and z axes in the orthorhombic group G_q are along $\underline{A}$ and $\underline{C}$ respectively, the y-axis being along $\underline{B}^*$ (orthogonal to $\underline{A}$ and $\underline{C}$).

The matrix representatives of the generators of G_q, say 2_x, 2_{1z}, $\bar{1}$ commute and have their squares equal to the matrix unity so that all irreducible representations Γ_j (j = 1, 2, 3, 4) of G_q are one-dimensional. On the other hand one finds easily the transformation properties of the small displacements u_1, v_1, w_1 of the atom 1 at 0 0 0 and u_2, v_2, w_2 of atom 2 at $0\ 0\ \frac{1}{2}$ under the operations of G_q. Primed letters u', v', w' characterize the displacements of the anions 1' at $\frac{1}{3}\ \frac{2}{3}\ \frac{1}{4}$ and 2' at $-\frac{1}{3} - \frac{2}{3} - \frac{1}{4}$. (When a point differs from the reference points by a lattice translation $\underline{t}$, its displacements are those of the reference point multiplied by $\exp 2\pi i \underline{q}.\underline{t}$. For instance the point $\frac{2}{3}\ \frac{1}{3}\ \frac{3}{4}$ differs from the reference point $2'(-\frac{1}{3} - \frac{2}{3} - \frac{1}{4})$ by the translation $\underline{t}$ = 1 1 1 so that its displacements are $(u', v', w')\ \exp 2\pi i \underline{q}.\underline{t} = (-u'_2, -v'_2, -w'_2)$). The following table 3 contains this information as well as the group characters of G_q.

TABLE 3. Representations of G_q and transformation properties of small displacements

Representations	Operators 1	2_x	2_{1z}	$2_x.2_{1z}$
Γ_1	+ 1	+ 1	+ 1	+ 1
Γ_2	+ 1	+ 1	- 1	- 1
Γ_3	+ 1	- 1	+ 1	- 1
Γ_4	+ 1	- 1	- 1	+ 1
Displacements				
$\underline{Mn}$	u_1	u_1	$-u_2$	$-u_2$
	v_1	$-v_1$	$-v_2$	v_2
	w_1	$-w_1$	w_2	$-w_2$
$\underline{P(As)}$	u'_1	u'_2	$-u'_2$	$-u'_1$
	v'_1	$-v'_2$	$-v'_2$	v'_1
	w'_1	$-w'_2$	w'_2	$-w'_1$

TABLE 4. Basis vectors belonging to Γ_{ju}

	for Mn			and	for P(As) displacements		
	U	V	W		U'	V'	W'
Γ_{1u}	$u_1 - u_2$	0	0		0	$v'_1 - v'_2$	0
Γ_{2u}	$u_1 + u_2$	0	0		$u'_1 + u'_2$	0	$w'_1 - w'_2$
Γ_{3u}	0	$v_1 - v_2$	$w_1 + w_2$		$u'_1 - u'_2$	0	$w'_1 + w'_2$
Γ_{4u}	0	$v_1 + v_2$	$w_1 - w_2$		0	$v'_1 + v'_2$	0

For saving place we have not listed the symmetry operations resulting from the multiplication by the inversion $\bar{1}$ which the reader may complete. It turns out that only the representations with $\chi(\bar{1}) = -1$, say Γ_{ju}, are to be considered. The basis vectors transforming according to the listed irreducible representations are obtained by the following summation over the symmetry operations Q (projection operator method).

$$\begin{pmatrix} U^{(\Gamma_j)} \\ V^{(\Gamma_j)} \\ W^{(\Gamma_j)} \end{pmatrix} = \sum_Q \chi^{(\Gamma_j)}(Q)\ Q \begin{pmatrix} u_1 \\ v_1 \\ w_1 \end{pmatrix} \tag{34}$$

For instance the characters in Γ_3 being + 1, - 1, + 1, - 1 for the respective symmetry operators Q : 1, 2_x, 2_{1z}, $2_x.2_{1z}$ and the corresponding displacements being v_1, $-v_1$, $-v_2$, $+v_2$ one has

$$V^{(\Gamma_3)} = +1.v_1 + (-1)(-v_1) + (+1)(-v_2) + (-1)(+v_2) = 2(v_1 - v_2) \tag{35}$$

The basis vectors listed in table 4 define the "displacement modes". For instance, the basis vectors belonging to Γ_{3u} are completely determined by making all other basis vectors (of Γ_{ju} with $j \neq 3$) equal to zero. In this particular case one has in

$$\Gamma_{3u} : v_2 = -v_1,\ w_2 = w_1 \text{ for Mn} ;\ u'_2 = -u'_1,\ w'_2 = w'_1 \text{ for P(As)} \tag{36}$$

2.3.3. Small displacements inferred from the similarity operators. We insert in

$$\underset{\sim}{R} = \underset{\sim}{S}\underset{\sim}{r} + \underset{\sim}{T} \tag{9}$$

the $\underset{\sim}{r}$ positions 4c) of the space group g = Pnma in the order we have adopted in earlier work (51)

$$\underset{\sim}{r} : (1)\ x, \tfrac{1}{4}, z\ ;\ (2)\ \bar{x}, \tfrac{3}{4}, 1-z\ ;\ (3)\ \tfrac{1}{2}-x, \tfrac{3}{4}, \tfrac{1}{2}+z\ ;\ (4)\ \tfrac{1}{2}+x, \tfrac{1}{4}, \tfrac{1}{2}-z \tag{37a}$$

and get the corresponding coordinate triplets of $\underset{\sim}{R}$ in the (hexagonal) reference frame of G

$$\begin{aligned}\underset{\sim}{R} : (1)\ & z-\tfrac{1}{4}, 2z-\tfrac{1}{2}, \quad x\ ;\ (2)\ \tfrac{5}{4}-z, \tfrac{3}{2}-2z, \quad \bar{x}\ ;\\ (3)\ & \tfrac{3}{4}+z, \tfrac{1}{2}+2z, \tfrac{1}{2}-x\ ;\ (4)\ \tfrac{1}{4}-z, \tfrac{1}{2}-2z, \tfrac{1}{2}+x.\end{aligned} \tag{37b}$$

For Mn we put

$$z_{Mn} = \tfrac{1}{4} - \xi\ ;\ x_{Mn} = \varepsilon \tag{38}$$

and find the following equations

$$\begin{aligned}R_1 &= 0\ 0\ 0 + (-\xi, -2\xi, \varepsilon)\ ;\ R_2 = 1\ 1\ 0 + (\xi, 2\xi, -\varepsilon)\\ R_3 &= 1\ 1\ \tfrac{1}{2} + (-\xi, -2\xi, -\varepsilon)\ ;\ R_4 = 0\ 0\ \tfrac{1}{2} + (\xi, 2\xi, \varepsilon)\end{aligned} \tag{37c}$$

Here we have split R_j into the equilibrium positions 2a) of G and the "small displacements". The comparison with the tabulated modes shows that the small displacements of Mn belong to the representation Γ_{3u}. The vector $-(\xi\underset{\sim}{A} + 2\xi\underset{\sim}{B})$ in atom 1(0 0 0) is perpendicular to $\underset{\sim}{A}$ and equivalent to the v_1 coordinate whilst $+\varepsilon$ is equivalent to w_1.

In the same way we put for P(As)

$$z_{As} = \tfrac{7}{12} - \xi'\ ,\ x_{As} = \tfrac{1}{4} - \varepsilon' \tag{39}$$

and find

$$\begin{aligned}R'_1 &= \tfrac{1}{3}\ \tfrac{2}{3}\ \tfrac{1}{4} + (-\xi', -2\xi', -\varepsilon')\ ;\\ R'_2 &= -\tfrac{1}{3}, -\tfrac{2}{3}, -\tfrac{1}{4} + 1\ 1\ 0 + (\xi', 2\xi', +\varepsilon')\ ;\\ R'_3 &= \tfrac{1}{3}\ \tfrac{2}{3}\ \tfrac{1}{4} + 1\ 1\ 0 + (-\xi', -2\xi', +\varepsilon')\ ;\\ R'_4 &= -\tfrac{1}{3}, -\tfrac{2}{3}, -\tfrac{1}{4} + 0\ 0\ 1 + (\xi', 2\xi', -\varepsilon')\end{aligned} \tag{37d}$$

Here the displacements $(-\varepsilon')$ of the reference atoms 1' and 2' (cf. R'_1 and R'_4) are the same so that $w'_1 = w'_2$ which assigns again the representation Γ_{3u} to the anion displacements. It is remarkable that there is no coupling of v' and w' coordinates in Γ_{3u}. However v displacements (say $\xi'(\underset{\sim}{A} + 2\underset{\sim}{B})$) are allowed by the group g. Thus we must conclude that the v' displacements belong to another representation of G_k . Figure 10 illustrates the displacement modes.

Remark. The displacements are restricted to be in the m_y plane of Pnma so that the u and u' modes which are orthogonal to m_y can be neglected altogether.

It has been brought to the attention of the author that the NiAs-MnP type transformation has been already discussed in the frame of the Landau theory of second order transformations (52). We hope that the conjugation of representation analysis and similarity operators will provide a useful tool for the study of transitions.

Remark. The matrices, constructed for each symmetry operator with the displacements, form a representation of the group which can be reduced by group theoretical technics. It can be

---

* If the displacements belonged to only one representations, ξ' would be strictly zero and $z(P, As) = \frac{7}{12}$ would be a "structural invariant".

shown* that

$$\Gamma = \Gamma perm \times V \tag{40}$$

where $\Gamma perm$ is the permutation representation and V the (polar) vector representation.

Last, but not least, an hamiltonian $\mathcal{H}$ can be constructed on the displacement modes. $\mathcal{H}$ is invariant in G_k

$$\mathcal{H} = - [aV^2 + bVW + cWW' + dVW'] - a'(V')^2 \tag{41}$$

is to be minimized under the constraints

$$V^2 + W^2 = \text{constant} = Z^2 \; ; \; (V')^2 + (W')^2 = \text{constant} = (Z')^2 \tag{42}$$

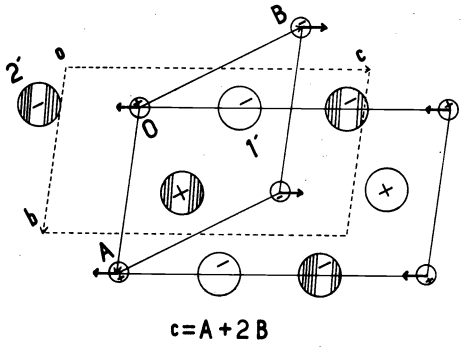

Fig. 10. MnP type displacement modes. Hexagonal cell $\underset{\sim}{A}$, $\underset{\sim}{B}$, origin 0 and orthorhombic cell $\underset{\sim}{b}$, $\underset{\sim}{c}$, origin o. The arrows indicate the cation displacements in the plane Z = 0. They are reversed in the plane Z = $\frac{1}{2}$.
The displacements along the hexagonal Z axis (= orthorhombic $\underset{\sim}{x}$ axis) are marked by + and - signs. They are the same in the planes Z = 0 and Z = $\frac{1}{2}$ for the cations and in the planes Z = $\frac{1}{4}$ and Z = $\frac{3}{4}$ for the anions.

2.3.4. Search of the subgroup g. The P subgroup of G must admit an orthorhombic lattice. As in the case of FeS, we proceed by steps of maximal subgroups. G = $P6_3/mmc$ admits a maximal subgroup Cmcm of index 3 which has the orthohexagonal (centred) translation lattice. The full notation of Cmcm is C^{mcm}_{bnn}. There are eight maximal subgroups of class mmm obtained by the loss of the translation $\frac{1}{2}\,\frac{1}{2}\,0$. One of them is Pmcn which in the standard notation of the International Tables becomes g = Pnma. The (orthorhombic) translation $-\frac{1}{2}\,\frac{1}{2}\,0$ coïncides with the translation $\underset{\sim}{B}$. The index of g in G is 6.

Remark. It is quite interesting to state that the image of g = Pnma in G (see table 2) would coïncide with G_k = Pmcm if in the glide plane operation $(m_z|1\;1\;\frac{1}{2})$ one could suppress the glide component 1 1 0. We shall investigate this point in another study (53).

2.4. Peierls instability and naive electron gas theory. Peierls (54) has shown that a one dimensional conductor of equally spaced atoms is unstable and that a gap is opened near k_F, or expressed otherwise the new "Fermi volume" $2k_F$ will just contain the conduction band and (on the low temperature side) an insulator or semi-conductor will be created.

In three dimensions one has in the theory of free electrons

$$N = \frac{1}{3\pi^2} k_F^3 \tag{43}$$

where N is the electron density (= number of electrons per unit volume and k_F the Fermi vector). If we put

$$k_F = 2\pi q_F \tag{44}$$

one has the simple formula

$$N = 2\left(\frac{4\pi}{3} q_F^3\right) \tag{45}$$

*see equation (1.14) in reference (37).

Here $\frac{4\pi}{3} q_F^3$ is the "Fermi volume" in the reciprocal space of the crystallographer. If we assume that the volume v* defined by the wave vectors g_1, g_2, g_3 which appear at the T_α transition of FeS just include the "Fermi volume"†

$$\frac{4\pi}{3} q_F^3 = (g_1 \times g_2).g_3 = v^* \tag{46}$$

one gets

$$N = 2v^*$$

or

$$Nv = 2 \tag{47}$$

Here $v = (\underset{\sim}{a} \times \underset{\sim}{b}).\underset{\sim}{c}$ is the unit cell volume in direct space and v* the unit cell volume in reciprocal space. Formula (47) just says that there are 2 conduction electrons in the volume v. Thus in FeS where v contains 12Fe atoms there would be 2 electrons per 12Fe say $\frac{1}{6}$ conduction electron per Fe atom so that FeS at high temperatures is a "poor" metal. The figure 11 shows the drop of the conductivity in FeS at $T = T_\alpha$ (11).

If we conjecture that the transition at 390 K in MnAs from the NiAs type to the MnP type is a metal-semiconductor transition, there would be 2 electrons per 4Mn atoms, say $\frac{1}{2}$ conduction electron per Mn atom in the metallic phase.

Remark. The cation lattice in NiAs type compounds, with its linear chains of equidistant atoms along $\underset{\sim}{c}$ seemed to offer a unique opportunity for "pairing effects" à la Peierls, but as we have seen the situation is more complexe in three dimensions and the cation displacements are mainly perpendicular to $\underset{\sim}{c}$ as well in FeS (below T_α) as in the MnP type.

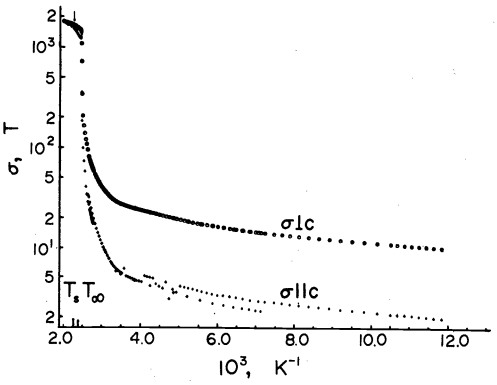

Fig. 11. Conductivity σ(T) versus T^{-1} in FeS (11). One notices the drop at T_α.

3. MAGNETIC ORDER IN PNICTIDES MX

In order to examine the occurrence of magnetic order we consider two species of series, the series MP where the cation varies : M = V, Cr, Mn, Fe, Co, Ni and the series CrX, MnX, FeX where the anion varies : X = P, As, Sb.

3.1. The MP series. Table 5 summarizes the information for the MP series, the number of valence and d electrons, theoretical values of the magnetization in the hypothesis of a strong ligand field (low spin configuration and all p anion orbitals filled) and the magnetization observed by neutron diffraction.

TABLE 5. Magnetic moments in MP

Compound	Valence electrons	d^n	Spin configuration	Moment observed in μ_B
VP	10	d^2	-	itinerant
CrP	11	d^3	-	"
MnP	12	d^4	↓ ↑↑↑	1.3
FeP	13	d^5	↓↓ ↑↑↑	0.41
CoP	14	d^6	↓↓↓ ↑↑↑	0.0
NiP	15	d^7		unstable

† this means that the first Brillouin zero identifies with the content of the Fermi surface.

The absence of any magnetic order in CoP is in favour of a low spin configuration.

The fact that VP and CrP show no magnetic order is ascribed to short metal-metal distances, producing "spin less" itineracy of d electrons (cf. Fig. 4) and broad metallic bands. All compounds MP have the MnP type structure with the exception of VP which is a metal crystallizing in the NiAs type (A = 3.18 Å, C = 6.22 Å ; note the high C/A ratio = 1.956, far above the "ionic" ratio of 1.63) and of NiP which is unstable below 850°C and crystallizes in an orthorhombic structure type with distortions even stronger than in the MnP type (55). Let us mention in this connection that NiAs is weakly paramagnetic and that the very short Ni-Ni distance of 2.514 Å (A = 3.61 Å, C = 5.028 Å) gives rise to strong metal-metal bonding. NiAs is metallic, but not superconducting down to 1.25 K (56). NiSb is metallic, diamagnetic, not superconducting down to 0.35 K (57) while NiBi, still NiAs type, is a superconductor with T_c = 4.25 K (58). The following molecular formulae give a feeling for the valency schemes

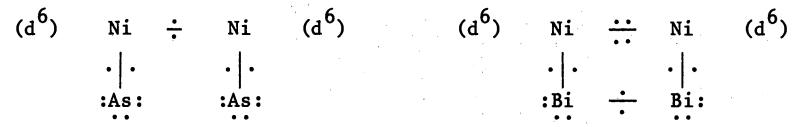

3.2. Elastic and magnetic energy. The main feature which stabilizes the NiAs structure with respect to other AB structures (rock salt, wurtzite, etc...) is the presence of short metal-metal distances (M-M) giving rise to M-M bonding which counteracts the Coulomb repulsion (59). In the crystallographic high temperature transition from the NiAs to the MnP type not only this short distance d_1 is conserved (M_1-M_2 in Kjekshus and co-workers (60a), M_1-M_4 in our notation (51)), but a new short distance d_2 is introduced (M_2-M_3 in Kjekshus, M_1-M_2 in our notation). Thus the driving force for the high temperature crystallographic NiAs → MnP transition is the establishment of new metallic bonds which favour spinless electron itineracy at low temperatures.

Inversely, if in a spinless itinerant situation one wants to get magnetic ordering, one must break the new metal bonds, say enlarge d_2 over a critical distance : one must overcome the MnP type deformation at least partly. The basis of the Rodbell-Bean theory of first order transitions (61) is the volume (or distance) dependence of exchange integrals. Thus we may expect first order transitions which either conserve the MnP type or even reach the stage of the NiAs type.

In the energy balance of the transition to magnetic order two factors are to be considered

i) the expense of elastic energy
ii) the gain of magnetic energy

The expense of elastic energy will be roughly proportional to the temperature at which the crystallographic (high temperature) transition MnP ⇄ NiAs takes place. The magnetic energy will be proportional to the square of the magnetic moment.

3.2.1. The CrX series. In CrP where d_1(2.768 Å) ≃ d_2(2.796 Å) the MnP type deformation is very strong and "there is no sign of a beginning transformation to NiAs type up to 1300 K" (46). The gain of magnetic energy is not sufficient to overcome the high elastic energy barrier and no magnetic order can take place.

In CrAs the crystallographic MnP → NiAs transition is observed at 1173 K (46) ± 20. The magnetic transition at T_N ≃ 260 K to an antiferromagnetic double helix is first order (60a) (51) (62) (63) and d_2 increases from 3.01 Å at 285 K to 3.14 Å (62) at 90 K. There is a large hysteresis effect so that the parameters of the non magnetic and the magnetic phases may be compared at the same temperature (62). The moment value is rather small (1.67 μ_B at 4.2 K). As the low site symmetry $\underline{m}$ lifts completely the degeneracy of the d electron levels, one may speculate that in the helimagnetic structures of MnP type, part of the d electrons are localized (or in narrow bands), part are still delocalized. In solid solutions CrP_xAs_{1-x} magnetic ordering breaks already down for x = 0.07. For x = 0.05, 0.10 and 0.20 the crystallographic NiAs → MnP transitions are at temperatures increased to 1230 K, 1270 K and 1350 K respectively (60b).

If As is replaced by the bigger anion Sb, the structure is of the NiAs type (A = 4.03 Å ; C = 5.463 Å) at any temperature. CrSb has a completely localized behaviour and nearly the full moment (2.84 μ_B at room temperature (64a) is observed in a structure which, as expected, is a collinear antiferromagnet. The Néel temperature is quite high T_N ≃ 720 K (64b) and the antiferromagnetism is due to the direct Cr-Cr exchange along C (the distance is 2.78 Å here and 2.68 Å in Cr_2O_3 in an analogous situation of face sharing octahedra).

One may prepare solid solutions $CrAs_{1-x}Sb_x$ which, at room temperature, are MnP type as long as the concentration of CrAs is above 59 %. At 4.2 K this limit moves to 42 % where T_N reaches its minimum value of 175 K.

Qualitative neutron diffraction studies above T_N show the absence of paramagnetic scattering in the forward direction for CrAs, but strong paramagnetic scattering for $CrAs_{0.5}Sb_{0.5}$ (65).

3.2.2. The MnX series. If in CrP one replaces Cr by a bigger cation like Mn, the spinless situation is removed. MnP is a ferromagnet between 78 K and 291 K and has a moment of 1.2 to 1.3 μ_B (extrapolated to 0 K) (66). Below 78 K one finds a nearly ferromagnetic double helix (67)(68), the magnetic moment remaining small (1.3 μ_B at 4.2 K). Unfortunately the author is not aware of any crystallographic study above and below T_c, but thinks that the transition at T_c should be first order. Also there does not seem to exist any crystallographic high temperature study of MnP itself.

In MnAs the temperature at which the crystallographic transition from the high temperature NiAs type to the MnP type takes place is only 393 K (47) much lower than in CrAs so that the elastic energies are in the ratio of 393/1173 ≃ 1/3 to the effect that in MnAs the gain of magnetic energy is more than sufficient to overcome the MnP deformation. Here the Mn-Mn distance d_2 jumps from 3.37 Å on the non magnetic side (MnP) to 3.722 Å on the ferromagnetic NiAs side (3.722 Å)(47). The magnetic saturation value of 3.4 μ_B (69) is confirmed by neutron diffraction (3.3 μ_B (47) at 4.2 K) and corresponds to a predominantly high spin state. It is also gratifying to state that above 400 K, one finds normal Curie-Weiss behaviour for the thermal variation of the inverse of the magnetic susceptibility, corresponding to 3.7 ± 0.2 μ_B (see fig. 4 in (70)). It is quite surprising that in the interval of 300 to 400 K where the "commensurate charge density wave of the MnP type" breaks in no electric resistivity measurements have been made. Figure 12 shows the phase equilibrium diagram (47).

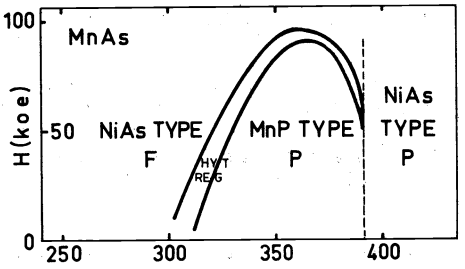

Fig. 12. Phase diagram of MnAs (field and temperature) after (47). Remark the large hysteresis region at the magnetic transition.

In MnBi, the ferromagnetic moment in the NiAs type structure is still higher, 4.5 μ_B at 5 K (71), which is ascribed to an orbital contribution (in fact the g-factor measured at - 180 C is about 2.4 (72)). When heating, there is a first order transition at 360 C to a state without magnetic moment (69). This high temperature structure can be quenched when stabilized by small amounts of Sb. Andresen et al. (73) could show that $MnBi_{0.9}Sb_{0.1}$ crystallizes in an orthorhombic lattice, close to orthohexagonal, as does MnP, but in a different space group which is $P222_1$. It should be noticed that, as Pmcn (Pnma), $P222_1$ is also a subgroup of Cmcm and thus a subgroup of index 12 of $P6_3/mmc$.

To summarize, all transitions from non magnetic to magnetic order, mentioned above, are first order.

The absence of magnetic order in MnP type compounds is as significant as its presence. For instance VAs (MnP type) does not show any magnetic ordering until the lowest temperatures investigated (74). The fact that there is no observable crystallographic transition to NiAs type at temperatures up to 1300 K indicates a high deformation energy. On the other hand the magnetic energy gain is too small in view of the small moment of V, compared to Cr or Mn.

One may also speculate that in very high fields CoAs or solid solutions $CoAs_{1-x}Sb_x$ could be switched to ferromagnetic with considerable volume effects.

3.3. Correlation between pressure, chemical substitution, transition temperatures and volume effects. In the same order of ideas, given a magnetic order in a MnP type compound, any physical effect which decreases the metal-metal distances, will bring the d electrons to a more itinerant situation. High pressure will destroy magnetic order in the sequence : ferromagnetism (or collinear antiferromagnetism) → helimagnetism → itinerant (spinless). The sign of dT_{trans}/dp, say of the variation of the magnetic transition temperature vs.pressure is that of $V_{upper} - V_{lower}$. When the upper state is spinless, this volume difference is negative. In CrAs one has dT_N/dp = - 19°/kilobar (65). When the upper state is paramagnetic, things are

different. For instance in $CrAs_{0.5}Sb_{0.5}$, V_{upper}(NiAs type) > V_{lower}(MnP type) (see fig. 1 in reference (51)) and consequently, one has $dT_N/dp = +16°/kb$ (65). These values, calculated in the frame of a first order transition (61) are in good agreement with experiment.

Substitution by smaller cations or anions produces the same effect as pressure. When FeP is added to MnP, the volume decreases regularly with the concentration t in $Mn_{1-t}Fe_tP$ (75). The Curie temperature T_c decreases gradually with t increasing, whereas the temperature of the transition ferro- to heli-magnetic T_{f-k} increases, starting from 50 K, until t = 0.12 is reached where T_c and T_{f-h} merge at 215 K (76). Assimilating the volume decrease to a pressure increase we conclude that in the range $0 < t < 0.12$ the difference $V_{non\ magn.} - V_{ferro}$ should be negative so that $dT_c/dp < 0$ whilst the difference $V_{ferro} - V_{helimagn.}$ should be positive so that $dT_{f-h}/dp > 0$. For $t > 0.12$, there is only one magnetic phase (helimagn.) present and T_N, measured by the maximum of the susceptibility plot, decreases from 215 K to 142 K at t = 0.3 so that here $V_{upper} - V_{lower} < 0$ or $V_{helimagn.} > V_{non\ magn.}$. These conclusions, based on the first order nature of the transition, have not yet been checked by experiment. (Unfortunately there are no experimental points between t = 0.3 and t = 1.00 where T_N = 125 K is reported (77)).

In the solid solution $Mn_{1-c}Fe_cAs$ (70) the effects are even more dramatic and can be checked. Here too the volume decreases with c increasing so that $dT_{trans.}/dc$ varies as $dT_{trans.}/dp$. On the MnAs rich side the solid solution is limited to $0 < t < 0.12$ for annealed samples. MnAs is ferromagnetic down to 0 K at ordinary pressure so that T_N (helimagnetism) would be, so to speak, negative. Here for c = 0.05 one observes at and below room temperature the MnP type structure and below T_N = 211 K a helimagnetic structure. One concludes that here $dT_N/dc > 0$ and $V_{upper} - V_{lower} > 0$. One has indeed V (293 K) = 127.7 Å^3 and V (95 K) = 120 Å^3 (78). At the same time the distance d_2 has decreased from 3.323 Å (293 K) to 3.084 Å (95 K) and the magnetic moment has switched from high to low spin (1.45 μ_B at 95 K). Thus the addition of a small percentage of FeAs has considerably increased the deformation of MnP type which fact is also visible from the increase of the temperature of the crystallographic transition MnP → NiAs to 673 K in a sample $Mn_{0.9}Fe_{0.1}As$ (79), to be compared to 388 K in MnAs. The propagation vector, "usually" along c (see figure 13), is here along a*. The same feature is found in $Mn_{0.95}Co_{0.05}As$ with T_N = 196 K. Here V (293 K) = 131.96 Å^3 and V (79 K) = 121.80 K. The d_2 distance varies from 3.40 Å at 293 K to 3.185 Å at 79 K, but the high spin situation is maintained (μ = 4.5 ± 0.3 μ_B) (80) so that the transition high → low spin should take place at a distance d_2 between 3.185 Å and 3.084 Å.

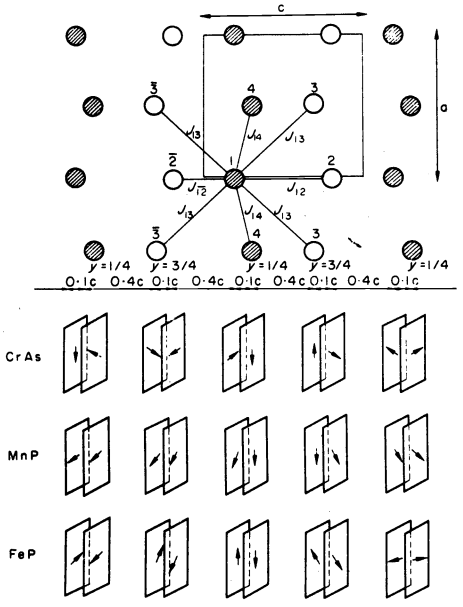

Fig. 13. Some usual double helix structures (after (51)).

*The interaction matrix procedure, developed in (51) can be easily adapted to this case.

Neither FeP nor FeAs which crystallize in the MnP type show any tendency to convert to NiAs type before they melt. Thus one can foresee high deformation energies, low magnetic transition temperatures (125 K (77) and 77 K (81) respectively), low magnetic energy gains in view of the smallness of the magnetic moment ($\sim 0.5\ \mu_B$) and consequently only small volume changes. Nevertheless let us assume that the transition from magnetic to non magnetic is first order and see if we find contradictions. In $FeP_{1-x}As_x$ a helimagnetic structure is reported for $w = 0.1$ with $T_N = 96$ K so that the transition temperature decreases with increasing As content and increasing volume (82). The same reasoning as above shows that dT_{trans}/dx and $V_{upper}-V_{lower}$ must be of opposite signs. Here $dT_N/dx < 0$ whence $V_{upper} - V_{lower} > 0$. With the parameters indicated in (82) one has V (293 K) = 94.08 Å^3 and V (80 K) = 93.85 K. The difference is small, but significant.

Thus we think that the conclusions and predictions of this paragraph are essentially correct. They are also in agreement with early high pressure work (83). However careful single crystal work might be able to transform somewhat our present views on "spinless" itineracy, based on powder data.

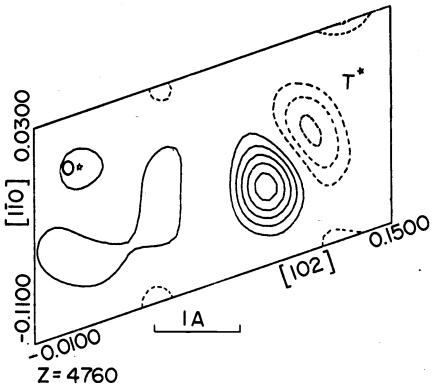

Fig. 14. Spin density map on oxygen in $Y_3Fe_5O_{12}$

Before I conclude I want to show you a last figure (Figure 14) obtained in our laboratory (84). It represents a spin density map in $Y_3Fe_5O_{12}$ where one has subtracted the spin densities localized on the tetrahedral (T) and octahedral (O) Fe atoms and marked by little stars. What is seen in the middle is the spin density transferred to the oxygene atom, say part of an antibonding orbital (cf. relation (1) of text). To visualize bonding and antibonding orbitals in sulfides and pnictides by appropriate X-ray and neutron techniques, looks today like a dream. But the dreams of today will be tomorrow reality.

REFERENCES

1. G. Hägg and A. L. Kindström, Z. Phys. Chem. (B) 22, 453 (1933).
2. E. F. Bertaut, P. Burlet and J. Chappert, Solid State Comm. 3, 335-338 (1965).
3. N. F. Mott, this conference.
4. J. A. Tossel, J. Chem. Phys. 66, 5712 (1977).
5. M. Wintenberger and J. L. Buevoz, Solid State Comm. 27, 511-513 (1978).
6. M. Wintenberger, B. Srour, C. Meyer, F. Hartmann-Boutron and Y. Gros, J. Phys. 39, 965-979 (1978).
7. B. Andron and E. F. Bertaut, J. Phys. 27, 619 (1966).
8. E. F. Bertaut, G. Roult, R. Aléonard, R. Pauthenet, M. Chevreton and R. Jansen, J. Phys. 25, 582-595 (1964).
9. J. Hubbard and W. Marshall, Proc. Phys. Soc. 86, 561 (1965).
10. J. T. Sparks, W. Mead and T. Komoto, J. Phys. Soc. Japan 17 B I, 249-262 (1962).
11. M. G. Townsend, J. R. Gosselin, R. J. Tremblay, A. H. Webster, J. Phys. Coll. C4 37, 11-16 (1976).
12. J. M. Coey, H. Roux-Buisson and R. Brussetti, J. Phys. Coll. C4, 1 (1976).
13. E. F. Bertaut, Bull. Soc. fr. Minér. Crist. 79, 276 (1956).
14. H. T. Evans, Jr., Science 167, 621-623 (1970).
15. R. C. Thiel and C. B. Van Den Berg, Phys. Stat. Sol. 29, 837 (1968).
16. E. Hirahara and M. Murakami, J. Phys. Chem. Sol. 7, 281 (1958).
17. A. Olés et al., Magnetic Structures Determined by Neutron Diffraction, Krakow, 423 (1976).
18. H. Vincent, Thèse d'Etat, Grenoble (1975).
19. H. Vincent, E. F. Bertaut and R. D. Shannon, Fifth Int. Conf. on Transition Metal Compounds, Collected Abstracts, Uppsala, Institute of Chemistry, 161-162 (1976).
20. R. D. Shannon and H. Vincent, Structure and Bonding 19, 1-44 (1974).
21. L. R. Walker, G. K. Wertheim and Jaccarino, Phys. Rev. Letters 6, 98-101 (1961).
22. J. B. Goodenough, Mat. Res. Bull. 13, 1305 (1978).

23. F. Jellinek, Inorganic Sulfur Chemistry Nickles, Elsevier, Amsterdam, (1968).
24. B. Lambert-Andron and G. Berodias, Solid State Comm. 7, 623-629 (1969).
25. J. Y. Henry, Thèse d'Etat, Grenoble (1976)
26. J. R. Regnard and J. C. Hocquenghem, J. Phys. Coll. C1 32, 268-269 (1971)
27. S. Hafner and M. Kalvius, Z. Kristallogr. 123, 443-458 (1966).
28. L. Levinson and J. Treves, J. Phys. Chem. Sol. 29, 2227-2231 (1968).
29. M. Tokonami, K. Nishiguchi and N. Morimoto, Amer. Mineralogist 57, 1066-1089 (1972).
30. L. M. Corliss, N. Ellott, J. M. Hastings, J. Appl. Phys. 29, 391 (1958).
31. M. Nishi and Y. Ito, Solid State Comm. 30, 551-574 (1979).
32. C. A. Tafi, R. Raj and J. Danon, J. Phys. Chem. Solids 36, 283-287 (1975).
33. A. W. Sleight and J. L. Gillson, J. Solid State Chem. 8, 29 (1973).
34. P. Imbert and M. Wintenberger, Bull. Soc. fr. Minér. Crist. 90, 299 (1967).
35. M. Wintenberger, B. Lambert-Andron and E. Roudaut, Phys. Stat. Sol. (a), 147 (1974).
36. M. G. Townsend, J. L. Horwood and J. H. Gosselin, Canad. J. Phys. 51, 2162 (1973).
37. E. F. Bertaut, J. Phys. Coll. C1 32, 462-470 (1971).
38. M. Wintenberger and A. Delapalme, Fifth Int. Conf. on Transition Metal Compounds, Collected Abstracts, Uppsala, Institute of Chemistry, 161-162 (1976).
39. M. Wintenberger, private communication.
40. I. E. Grey, J. Solid State Chem. 11, 128 (1974).
41. I. E. Grey, private communication.
42. E. F. Bertaut and Y. Billiet, C. R. Acad. Sc. Paris 287, série A, 989-991 (1978).
43. E. F. Bertaut and Y. Billiet, Acta Cryst. A (1979) under press.
44. International Tables for Crystallography, Int. Union of Cryst. to be published in 1980.
45. Y. Billiet, Acta Cryst. A 34, 1023-1025 (1978).
46. K. Selte and A. Kjekshus, Acta Chem. Scand. 27, 3195-3206 (1973).
47. A. Zieba, K. Selte, A. Kjekshus and A. F. Andresen, Acta Chem. Scand. A 32, 173-177 (1978)
48. E. F. Bertaut, Helv. Phys. Acta 41, 683-692 (1968).
49. E. F. Bertaut, Proc. of the Eur. Meeting on Ferroelectricity, Saarbrücken, (1969), Editor Wissenschaftliche Verlagsgesellschaft, Stuttgart, 7-21 (1970).
50. E. F. Bertaut, Acta Cryst. A 24, 217 (1968).
51. A. Kallel, H. Boller and E. F. Bertaut, J. Phys. Chem. Sol. 35, 1139-1152 (1974).
52. H. F. Franzen, C. Haas and F. Jellinek, Phys. Rev. B 10, 1248-1251 (1974).
53. E. F. Bertaut, to be published.
54. R. E. Peierls, Quantum Theory of Solids, Oxford, Clarendon Press (1955).
55. E. Larsson, Arkiv Kemi 23, 325 (1965).
56. B. T. Matthias and J. K. Hulm, Phys. Rev. 92, 874 (1953).
57. T. H. Geballe and V. B. Compton, Rev. Mod. Phys. 35, 1 (1963).
58. G. S. Zhdanov and R. N. Kuzmin, Soviet Phys. Cryst. 5, 532 (1961).
59. J. B. Goodenough, Magnetism and the chemical bond, Interscience and John Wiley, N.Y. (1963).
60a K. Selte, A. Kjekshus, W. E. Jamison, A. F. Andresen and J. E. Engebretsen, Acta Chem. Scand. 25, 1703 (1971).
60b K. Selte, H. Hjersing, A. Kjekshus and A. F. Andresen, Acta Chem. Scand. A 29, 695-698 (1975).
61. D. S. Rodbell and C. P. Bean, J. Appl. Phys. 33, 1037 (1962).
62. H. Boller and A. Kallel, Solid State Comm. 9, 1699 (1971).
63. N. Kazama and H. Watanabe, J. Phys. Soc. Japan 30, 1319 (1971).
64a T. R. Mc Guire, Bull. Am. Phys. Soc. SII 8, 55 (1963).
64b A. I. Snow, Phys. Rev. 85, 365 (1952).
65. A. Kallel, Thèse d'Etat, Grenoble (1972).
66. C. Guillaud, C. R. Acad. Sc. Paris 235, 468 (1952).
67. J. B. Forsyth, S. J. Pickart and P. J. Brown, Proc. Phys. Soc. (London) 88, 333 (1969).
68. G. P. Felcher, J. Appl. Phys. 37, 1056-1058 (1966).
69. C. Guillaud, J. Phys. Rad. 12, 233 (1951).
70. K. Selte, A. Kjekshus and A. F. Andresen, Acta Chem. Scand. A 28, 61-70 (1974).
71. A. F. Andresen, W. Hälg, P. Fischer and E. Stoll, Acta Chem. Scand. 21, 1543 (1967).
72. G. D. Adam and K. J. Standley, Proc. Phys. Soc. (London) A 66, 823 (1953).
73. A. F. Andresen, J. E. Engebretsen and J. Refsnes, reported in Thesis Andresen A.F., Kjeller (1971).
74. K. Selte, A. Kjekshus, A. F. Andresen, Acta Chem. Scand. 26, 4057-4062 (1972).
75. J. Bonnerot, R. Fruchart and A. Roger, Phys. Letters 26 A, 536-537 (1968).
76. A. Roger and R. Fruchart, C. R. Acad. Sc. Paris 264, 508-511 (1967).
77. G. P. Felcher, F. A. Smith, D. Bellavance and A. Wold, Phys. Rev. B 3, 3046-3052 (1971).
78. K. Selte, A. Kjekshus, P. G. Peterzens and A. F. Andresen, Acta Chem. Scand. A 30, 671-672 (1976).
79. K. Selte, A. Kjekshus and A. F. Andresen, Acta Chem. Scand. 27, 3607-3608 (1973).
80. K. Selte, A. Kjekshus, G. Valde and A. F. Andresen, Acta Chem. Scand. A 30, 468-474 (1976).
81. K. Selte, A. Kjekshus and A. F. Andresen, Acta Chem. Scand. A 26, 3101-3113 (1972).
82. K. Selte, A. Kjekshus, T. A. Oftedal and A. F. Andresen, Acta Chem. Scand. A 28, 957-962 (1974).
83. J. B. Goodenough and J. A. Kafalas, Phys. Rev. 157, 389 (1967).
84. M. Bonnet, A. Delapalme, P. Becker and H. Fuess, J. of Magn. and Magnetic Mat. 7, 23-25 (1978).